AIAA SciTech Forum
8–12 January 2018, Kissimmee, Florida
2018 AIAA Spacecraft Structures Conference

10.2514/6.2018-1678

Flight Build of a Furled High Strain Composite Antenna for CubeSats

Kevin Cox[1], Bruce Davis[2], Ryan VanHalle[3], Will Francis[4]
Roccor, Longmont, Colorado, 80503

In Q2, 2016 Roccor was tasked to develop a CubeSat antenna mechanism that deploys four large radial petals from a small, 2U stowed volume. It was determined that High Strain Composites (HSC) coupled with a copper-beryllium alloy enabled a simplistic furled solution utilizing few mechanical parts. Laminate architecture optimization was performed with a primary goal to maximize deployed frequency with a minimum laminate thickness, mass and susceptibility to creep. However, due to the high strains imparted while stowed, creep effects caused significant deformation to the petal laminate once deployed. A top-level creep-recovery investigation was performed including fabrication of copper-beryllium/fiberglass-epoxy laminates, long-term creep durations at high temperature, and subsequent measurement of the recovery rate. It was found that a combination of laminate characterization and design tweaks were suitable to meet requirements. This paper describes the design, test and qualification of two flight systems at Roccor over the course of a nine-month development period.

I. Nomenclature

A	= area
C	= circumference
D_{11}	= laminate bending stiffness
E	= modulus of elasticity
F	= force
h_c	= crept height
h_k	= distance from laminate mid-plane to top of ply
h_{k-1}	= distance from laminate mid-plane to bottom of ply
h_r	= recovered height
I	= area moment of inertia
k_2/k_1	= change in reaction rate per change in temperature
L	= length
P	= pressure
$\bar{Q}_{11}$	= axial ply stiffness
R	= laminate region
r	= bend radius
T_{Hot}	= elevated creep temperature
T_{RT}	= room temperature creep temperature
$t_{@RT}$	= equivalent creep duration at room temperature
$t_{@Hot}$	= creep duration at high temperature
U	= strain energy
V	= volume
w	= laminate width
ΔT	= change in temperature for reaction rate
Ø	= Outer diameter of furled petals

[1] Senior Mechanical Engineer, Roccor, 2602 Clover Basin Dr, Longmont, Colorado 80503
[2] Principal Engineer, Roccor, 2602 Clover Basin Dr, Longmont, Colorado 80503, AIAA Senior Member
[3] Manufacturing Engineer, Roccor, 2602 Clover Basin Dr, Longmont, Colorado 80503
[4] VP Engineering, Roccor, 2602 Clover Basin Dr, Longmont, Colorado 80503, AIAA Senior Member

II. Introduction

THE emergence of the small satellite platform and subsequent ease of access to space has created high demand for advanced, yet compact spacecraft systems serving a range of science, commercial and defense applications. Furthermore, the industry-wide embracement of the CubeSat standard, establishing both spacecraft form factor and consistent launch requirements, has established investment in off-the-shelf spacecraft components and high quantity production within the field. Across the community, one of the largest hurdles to developing a successful CubeSat system is the challenge in miniaturizing the technology to function within the desired form factor. This is especially challenging when designing deployable structures such as large antennas or solar arrays, where common physical components such as fastened interfaces, articulated joints and actuators are not efficient in the miniaturized form factor. Furthermore, structural performance does not often scale linearly in size causing the need to embrace different architectures at smaller scales to enable a desired deployed stiffness and precision. One such technology receiving increased attention within the CubeSat community are High Strain Composites (HSC) or materials that deform from one shape to another during deployment. A commonly known high strain device is a slit-tube, or a deployable "tape-measure" boom that allows the cross section to be flattened and rolled into a coil reaching a high packaging efficiency. Although the metallic slit-tube device has extensive flight heritage, a controlled deployment requires complex mechanisms to control the strain energy of the wrapped coil. When fabricating a slit-tube boom with a HSC, the ability to tune the composite laminate to control the strain energy of the furled structure offers a new level of simplicity while enabling adequate control to deploy and retract the device. The use of HSCs offer an improved level of mechanism simplicity over architectures utilizing traditional moving mechanisms such as rotational joints, springs, dampers and latches.

Roccor LLC, of Longmont Colorado was approached in Q3 of 2016 by an advanced CubeSat payload provider to design a deployment mechanism that would unfold a series of co-planer RF elements on orbit. This customer required a rapid project development ranging from early requirements definition to the delivery of multiple flight units over the course of a 9 month period. To add to the challenge, this effort was bounded by a relatively small budget which drove the need for mechanism simplicity and limited redundancy. The desired RF elements consisted of four petals, each measuring roughly 20" x 5" in length and height respectively that are aligned radially about a central hub. These petals would also need to be wrapped or folded to be stowed within a 2U CubeSat form factor. The geometry of this antenna system is shown in Fig. 1 with the four petals shown in the deployed state. Here the co-planer petals are shown in green, and the desired stowage volume of 10x10x20 inches is shown in purple. The remaining 6U CubeSat volume is identified with a semi-transparent box.

Structurally, the deployed petals needed to maintain a stiffness requirement above 0.5 Hz, a lateral precision of +/- 4" at the petal distal edge and a twist precision of 1" measured with respect to the top/bottom of the outer ends. It was found that the simplest approach was to wrap the four petals around a central hub and utilize strain energy to deploy upon the release of a perimeter restraining band. The petals, consisting primarily of a copper to enable RF performance, were reinforced with high strain composite lamina to control the stowed strain energy and deployment dynamics. The added lamina also protected the metallic RF element while stowed and improved the deployed structural performance. In this paper, the end-to-end development process of the petal design is discussed at length; this includes the architectural trades, laminate fabrication, early challenges such as delamination and creep effects, and finally the integration efforts of this system into the spacecraft deployment mechanism. The complete deployment system was integrated and tested in Q2 of 2017 and maintains an expected flight date in early 2018.

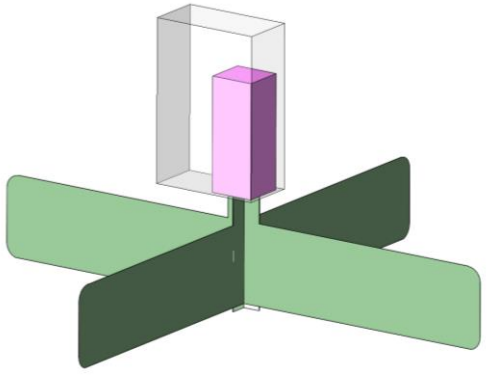

Fig. 1 Basic geometry of deployed CubeSat antenna

III. Architectural Trade and Laminate Design

The challenge of deploying a series of large, furled flat panels within a small CubeSat form factor was broken down into several targeted areas for the Roccor team to work through. The first, and primary focus of this paper, consisted of designing a laminate that could withstand the high strains while stowed, ensure sufficient energy for a robust deployment and finally provide adequate stiffness and precision once exposed. Important considerations such as defining the furled geometry of the petals were a central focus, especially in the transition region between the furled panels and the central petal supporting structure. The second category focused on the mechanics for how to stow, package and protect the furled petals within the CubeSat volume during launch, and upon activation, release the petals in the space environment. This area had the added complexity of physically moving the stowed petals from the cocooned volume to the outside of the spacecraft prior to petal extension. In addition, the deployment synchronization and analysis of the petal unfurling were prime focus areas within this group. The final category consisted of the electrical considerations such as the incorporation of the actuation device, integration of the RF electronics, wire harness management and finally, providing sensory feedback indicating a successful deployment.

The first step in the design of the petal, was to define the key geometric constraints imparted by the CubeSat envelope and central hub structure. This latter component, supplied by the payload provider, consisted of two interlocking plates forming a cross, with each of the petals bonded to the exposed outboard surfaces. This rigid structure had a diameter of 2.6" and contained finely tuned RF elements and electronic components, requiring delicate care. This geometry is shown as the light green components in Fig. 2 below. The RF petals extended beyond the interlocking plates and were geometrically required to sustain a ~0.25" bend radius as they transitioned from the central hub structure to the larger, wrapped geometry required of the 2U CubeSat form factor. This immediate region, defined as the transition area, contained the highest strain within the system design. Finally, the petal length and spacecraft envelope of ~3.1" square required each petal to be wrapped just over two full rotations around the central supporting structure with a maximum petal thickness of 0.020". Further considerations were imparted to maximize volume such as a non-circular wrapping geometry and the clocking of the central hub with respect to the space envelope to maximize the transition area bend diameter. This geometry is further described in Fig. 2.

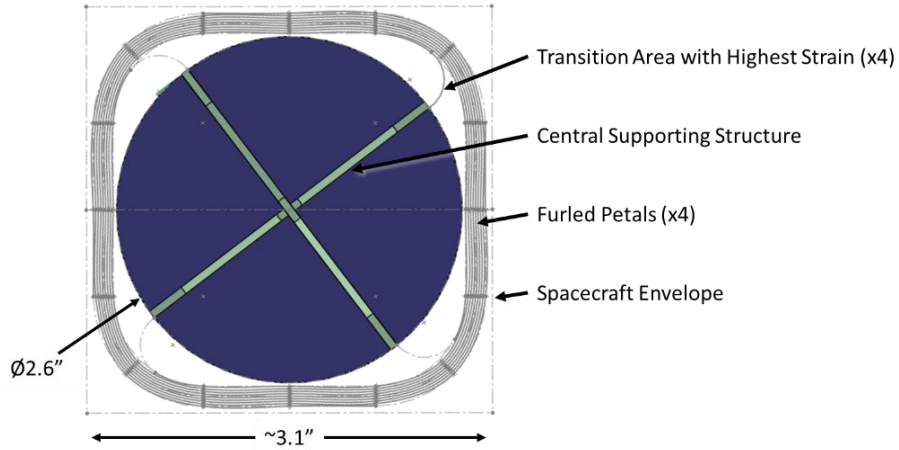

Fig. 2 Basic geometry of deployed CubeSat antenna

The initial petal laminate design consisted of a homogenous approach where the central RF conducting element was sandwiched with reinforcing lamina across the entire petal length. Here the RF element was baselined to be Copper Beryllium (CuBe) due to its excellent electrical conductive performance and ability to withstand high strains. Several lamina materials were considered, however E-glass was set as the baseline due to the material's high strain capability, availability and low cost. Upon early modeling and coupon fabrication, it was quickly determined that a variation of laminate designs across the length of the petal was required to optimize performance. For example, it was found that reinforcing the outer 1/3rd of the petal geometry did not increase deployed stiffness, shown on the left side of Fig. 3 in light blue (marked CuBe). When reinforcing this area, the added mass of the lamina at the distal end overpowered the benefits of the improved localized stiffness resulting in an overall lower frequency. It was also found that this added distal mass reduced the 1g buckling resistance, a property that made ground testing more difficult. In addition, the increased thickness of a reinforced outer petal region added to the overall wrapped diameter that imparted additional requirements on the remainder of the deployer design. Along the first 2/3^{rds} of the deployed petal, it was

found beneficial to taper the laminate in order to rigidize the base while also keeping the mass as close to the root as possible. Due to strain considerations, the maximum reinforcement considered across this region of the petal was the CuBe center element sandwiched between two layers of E-glass lamina, shown as Region 1 (R1) in Fig. 3. This tapered to a single layer of lamina across a region roughly 2/3^{rds} away from the root and is noted as Region 2, (R2) in Fig. 3. Finally, Region 3 (R3) was bare CuBe, and for reasons discussed later, special considerations were taken in the transition area, noted as Region 0 (R0) in Fig. 3. The lengths of each region, L_A, L_B and L_C were optimized for reduced mass and thickness while increasing deployed stiffness via finite element software. In addition to the spanwise laminate optimization, studies were also performed to investigate the dependency of structural performance on chord-wise laminate height. Laminate modifications similar to those described above, i.e.: ply drop thickness and location with respect to the upper and lower petal edges were implemented and were dependent on the system RF performance.

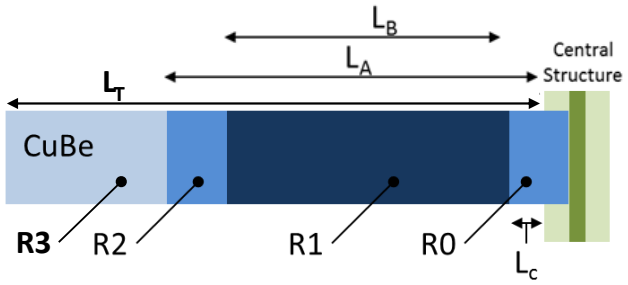

Fig. 3 Petal laminate design: R0 and R2 consisted of single layers while R1 contained multiple layers of HSC reinforcement

With the goal to balance performance between petal deployed frequency, 1g buckling resistance, thickness and tolerance to creep, a basic laminate design was established to include a central CuBe layer of thickness 0.003" that was sandwiched between either one or two layers of 0-90 E-glass. Initially within the design, the CuBe and available lamina materials were sized to ensure adequate strain margin. Fig. 4 below shows the calculated performance of the CuBe and E-glass lamina layers (bent to a 0.25 in radius) with the light green areas displaying the capacity of the material while the sloped line reflects the anticipated strain of each lamina layer (top and bottom).

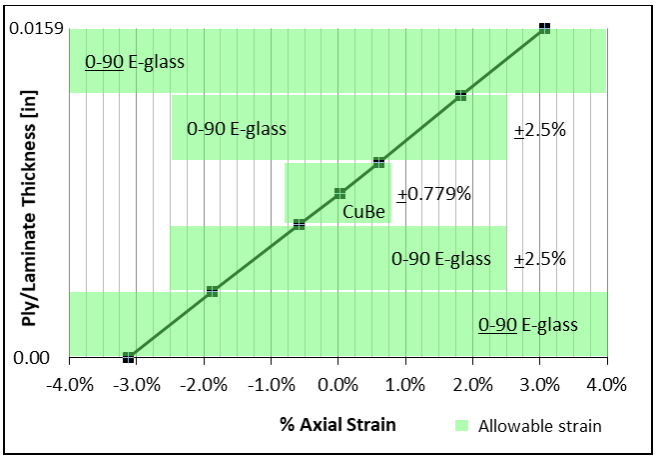

Fig. 4 Petal laminate design: R0 and R2 consisted of single layers while R1 contained multiple layers of HSC reinforcement. Strains reflect 0.25 in radius bend

While the FEM solver was able to easily optimize the petal design parameters L_A and L_B based on petal frequency, thickness, and 1g buckling resistance, the susceptibility to creep required more detailed analysis. Here the concern related to the deployed distal precision requirements of ±4 inches with respect to the orientation of the central hub structure. Of particular note was region R0 and the corresponding L_C parameter which needed to bend to a 0.25 inch radius and thus experienced the highest strain within the system. In addition R1 had unique challenges as it also experienced higher strains due to the multiple lamina layers and long distance across the petal.

Region R0

During initial studies, this region consisted of two laminas on each side of the CuBe material to maximize petal stiffness and attachment to the central hub. However upon early coupon testing, it was found that the laminate was not robust to numerous bending cycles as early signs of debonding developed after extensive handling. In addition, it was found that the outer lamina, initially oriented at ±45 deg to improve 1g stability, were prone to large creep effects when subjected to high strains. Upon testing a full length petal, the R0 region contributed to the majority of the distal end deflection due to creep. As such, upon further analysis, it was found that eliminating the outer lamina over the R0 transition region did not significantly reduce the deployed stiffness, however it yielded significant benefits in petal robustness and deployed precision.

Region R1

As mentioned above, the outer E-glass lamina were initially oriented at ±45 deg to improve 1g stability. While this region was strained to a significantly lower magnitude than R0, (minimum bend radius of 1.3 inches), it remained robust throughout testing. However, the large extended area defined by L_B amplified small creep effects and significantly degraded the deployed distal precision. It was found mid-way through system design that the change in orientation from ±45 deg to 0-90 deg plies dramatically reduced creep effects in this region. Table 1 below shows the change in deployed performance when rotating the outer lamina from ±45 deg to 0-90 degs.

Table 1: Impacts to deployed petal performance with lamina orientation at ±45 deg and 0-90 deg

Design	R1 laminate layup	Nat freq., Hz	1g stability	Furled force (stored energy)
Initial	$[\pm 45/0\text{-}90/CuBe_{1/2}]_s$	0.594	1.22	8.5 lbf
Final	$[0\text{-}90/0\text{-}90/CuBe_{1/2}]_s$	0.629 (+6%)	0.94 (-23%)	9.8 lbf (+16%)

In Table 1, the "1/2" subscript indicates a half-layer of CuBe, and the subscript "s" refers to a symmetric laminate. The values given for 1g stability represent the number of g's that the structure can withstand before buckling. This was not a hard system requirement, so a reduction in stability for the Final design was acceptable given the improvements in creep resistance and natural frequency.

Furled strain energy

Having determined the optimized laminate (and petal geometry), the challenge of restraining the furled antenna became the next challenge. More specifically, the objective was to determine the force required to hold the four petals in their furled shape. The design intent was to restrain the furled petals with a strap or tether that was flexurally compliant yet rigid in the hoop-wise direction. Sizing of the strap and a number of other deployment characteristics and mechanisms were thus dependent on the holding force.

A close-formed solution was developed to calculate the strain energy of the four petals including spanwise variations in petal width, laminate design (layup and ply drop locations), and strain. For an isometric material, the stored energy is calculated with Eq. (1) where *EI* is the bending stiffness, α is the angle through which the plate is bent, and *L* is the plate length. For quasi-isotropic materials like the CuBe/E-glass composite, the equation must be modified to take into account for the ply thicknesses and stacking sequence: thus taking the form of Eq. (2) and including the plate width, *w*, and the bending stiffness D_{11} which is based on laminate theory and readily explainable in any textbook on composite materials, i.e. [3].

$$U = \frac{\mathrm{EIL}}{2r^2} \tag{1}$$

$$U = \frac{D_{11} w \mathrm{L}}{2r^2} \tag{2}$$

$$D_{11} = \frac{1}{3}\sum_{k=1}^{n}(\bar{Q}_{11})_k(h_k^3 - h_{k-1}^3) \tag{3}$$

The $\bar{Q}_{11}$term represents the axial (x-axis) stiffness, h_k and h_{k-1} are equal to the distances from the laminate mid-plane to the top and bottom surfaces of the ply k respectively; k = 1 is the first ply laid down, k = 2 is the second and k = n is the last ply laid down. As an example, region R2 would be described as follows: k = 1 is the E-glass ply at the inner diameter, k = 2 is the CuBe layer, and k = 3 is the E-glass ply at the outer diameter. The laminate bending stiffnesses (D_{11}) were calculated individually for regions R0 – R3, and the closed form solution for stored energy in a single petal took the form of Eq. (4).

$$U = \sum_{R=0}^{3} U_R = \sum_{R=0}^{3} \frac{D_{11.R} * w_R * (L_{R+1} - L_R)}{2 * r_R^2} \quad (4)$$

The energy stored in each region of the stowed petal is presented in Table 2 along with values/relations for the other variables. The width column in the table uses 'x' to represent the spanwise length variable. The stack-up of laminate thickness after the 1st revolution coincided very nearly with the ply drop at the R1-R2 transition.

Table 2: Calculated strain energy in a single furled petal

Region, *R*	Bending stiffness, D_{11} [Nm]	Width *w* [m]	Length, *L* [m]	Bend radius, *r* [in, m]	Energy, *U* [Nm]
0	$D_{11.0} = 0.0307$	$w_0 = w_0(x)$	$L_{R0} = L_C$	$r_0 = 0.25, 0.064$	0.968
1	$D_{11.1} = 0.1025$	$w_1 = w_1(x)$	$L_{R1} = L_B$	$r_1 = 1.55, 0.394$	1.594
2	$D_{11.2} = 0.0307$	$w_2 = w_2(x)$	$L_{R2} = L_A - L_B - L_C$	$r_2 = 1.57, 0.398$	0.084
3	$D_{11.3} = 0.0052$	$w_3 = w_3(x)$	$L_{R3} = L_T - L_A$	$r_3 = 1.57, 0.398$	0.050

The stored energy of four stowed petals was readily calculated by summing Regions 0 – 3 and multiplying by four to yield 10.8 Nm. A conservative approach was taken assuming zero friction between the petals and the strap; thus the stored energy of the petals was completely contained within the volume of the strap and Eq. (5) was used to find the required force: where A = cross section area of the strap, C = length of the strap and Ø = 3.1 in (outer diameter of the furled petals).

$$U = P * V = \frac{F}{A} * CA = F\pi\emptyset \quad \rightarrow \quad F = \frac{U}{\pi\emptyset} \quad (5)$$

The restraining force was thus equal to 9.8 lbs. During system integration and testing, the restraining force was experimentally measured to be between 10 and 11 lbs for all systems built. Considering the large strains in the petals, the accuracy of the (linear) analytical solution was quite high, predicting to with 10% of the solution.

IV. Petal Fabrication & Coupon Testing

Following the petal layup analysis and optimization, the focus turned to quantifying the creep and recovery performance of the petals after a system requirement of 1 year stowage at room temperature. The first challenge however was to fabricate coupons that could actually achieve the flexural strain required by the design. A main assumption in the preceding section was that all plies were perfectly bonded together. However, initial attempts to bend the fabricated coupons resulted in delaminations between the CuBe and glass fiber plies as shown in Fig. 5. Delamination was found on both the tensile and compressive sides and often occurred below the design strain. After experimenting with various surface cleaning and abrading techniques, the issue remained. Therefore an alternative approach was taken to improve the surface finish by applying a black oxide coating to the CuBe similar to that described in [4]. The improvement in adhesion was an immediate success and all coupons and petal builds thereafter implemented the black oxide treatment.

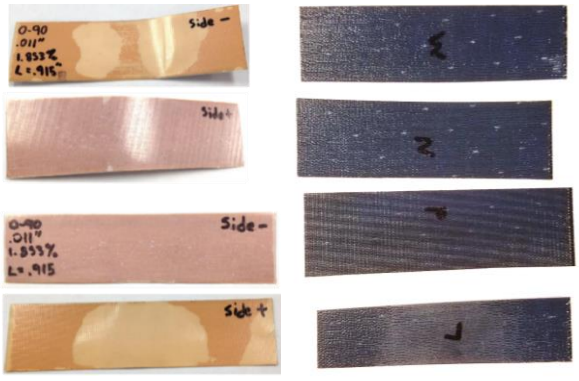

Fig. 5 Surface-abraded coupons experienced delamination after flexure due to poor adhesion between CuBe and glass fiber plies (left column), coupons treated with black oxide achieved a superior bond (right column)

Considering the high strains inherent in the furled petals during stowage, the creep resistance and recovery of the Copper-beryllium/fiberglass-epoxy composite was of interest. Moreover, system design requirements specified a maximum deployed tip precision of ±4 in from straight. Naturally, creep data describing a composite of this type and loaded in high-strain flexure was not available in previous literature; typically data is only available for more homogenous materials loaded axially and subjected to constant load (stress) instead of constant strain. Therefore a material characterization campaign was developed to get a first order understanding of creep and recovery of the composite. The goal was to use the experimental creep-recovery response of the material to first, estimate the amount of creep experienced by the petal after 1 year of stowage, and second, to understand how much the material recovered and at what rate. The test plan focused on only the R0 region which had the highest influence on the tip deflection because (1) this region experienced the largest strain and (2) being located at the root, any small amount of creep/deflection here would be significantly magnified out at the tip of the petal.

By taking advantage of the time-temperature dependency inherent in the laminate epoxy, the creep tests were conducted at elevated temperatures (71.4° C) to maintain the project schedule. Eight $[0\text{-}90/CuBe_{1/2}]_s$ coupons were fabricated and subjected to 2% strain by being wrapped around a 0.25 in radius bend. Four creep test durations were studied (1 hour, 3 hours, 21 hours and 90 hours); each included two coupons. Two additional coupons were created for long-term room temperature testing, however data was not available until well after the hardware was delivered. At the end of each creep test, the coupons were quickly removed from high temperature and their residual deflections measured in a manner similar to [5] and [6], where the measurement was the distance (height) from the unloaded position (horizontal) to the current position as shown in Fig. 6. The first measurement for each sample was taken 1 minute after removal of the flexural displacement, and additional measurements were taken periodically afterwards to characterize the recovery response at room temperature. The height values measured for the samples were extrapolated to the full petal length to give an estimation of tip deflection due to creep in the 0.25 in radius bend (R0).

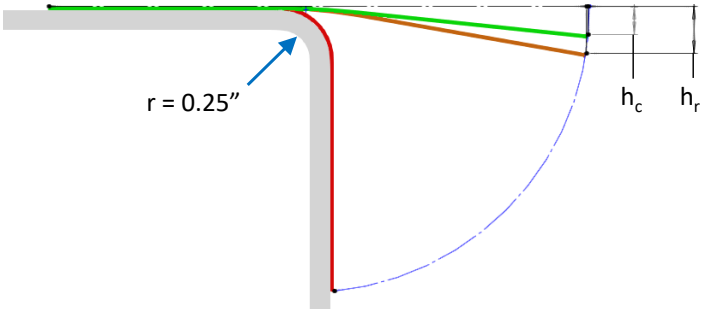

Fig. 6 Coupon flexure during high-temp creep (red), after release of flexure constraint (orange) and after recovery (green)

Results for residual creep (converted to tip deflection as described above) are plotted as a function of recovery time (in hours) for each creep duration in Fig. 7. The results produced logarithmic regressions summarized in Table 3 and resulted in a linear plots with a log-scale x-axis: a common attribute of both creep and recovery studies. After the high temperature exposure, the material did not show any signs of discoloration, swelling/shrinking, embrittlement, or other signs of degradation.

Fig. 7shows a higher tip deflection (creep) and steeper (faster) recovery from longer creep duration curves. This is consistent with expectations because as the material creeps more and more, the back-stresses (recovery stress) in glass fiber plies and the strain energy in the CuBe both become larger.

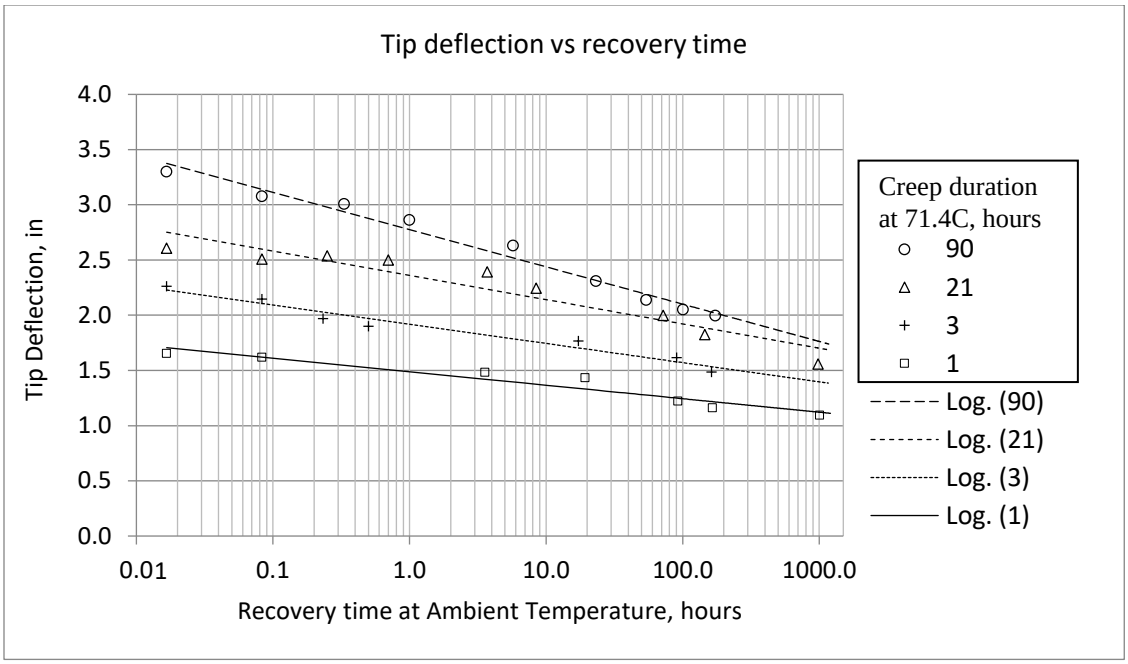

Fig. 7 Tip displacement from high temperature creep durations versus recovery time

Table 3: Logarithmic regression equations for each creep duration

Creep Time at 71.4°C (hours)	Logarithmic regression
1	-0.0531*LN(x)+1.4885
3	-0.0756*LN(x)+1.9187
21	-0.0955*LN(x)+2.3612
90	-0.1466*LN(x)+2.7751

By rearranging the results in Fig. 7, it was possible to create a relationship directly between creep duration (petal stowage time) and initial (after 1 minute) and recovered (after 200 hours) tip deflection. The 200 hour recovery time (~8 days) was determined to be a realistic timescale with respect to mission operations to allow for petal shape recovery after deployment. For this data to be meaningful however, the dwell times at 71.4°C first needed to be shifted into creep time at room-temperature. In determining the time-temperature shift, a simplified approach was taken since limited test data was available; the Arrhenius equation was implemented and rearranged to the form in Eq. (6), common for accelerated aging studies. The results are plotted in Fig. 8.

$$t_{@RT} = t_{@Hot}\left(\frac{k_2}{k_1}\right)^{\frac{T_{Hot}-T_{RT}}{\Delta T}} \tag{6}$$

Equation (6) yields the equivalent creep duration at room temperature ($t_{@RT}$ = 22°C) given a creep duration at hot temperature ($t_{@Hot}$ = 1, 3, 21, 90 hours), the change in rate of reaction (k_2/k_1) per change in temperature (ΔT = 10°C), and the difference between the high temperature and room temperature. k_2/k_1 is an experimentally derived value that was not investigated during this project. A common value for k_2/k_1 in polymers is 2 [7], but this assumes a homogenous material which was not the case for the antenna petal laminate. Since the glass fibers and CuBe are less sensitive to creep than the epoxy matrix, then a doubling of the reaction rate would represent the upper bound for what the coupon could exhibit. Likewise, a temperature independent reaction rate (k_2/k_1 = 1) sets the lower bound for how the coupon could react. Hence, the upper and lower limits for the time-temperature shift were created to bound the estimation.

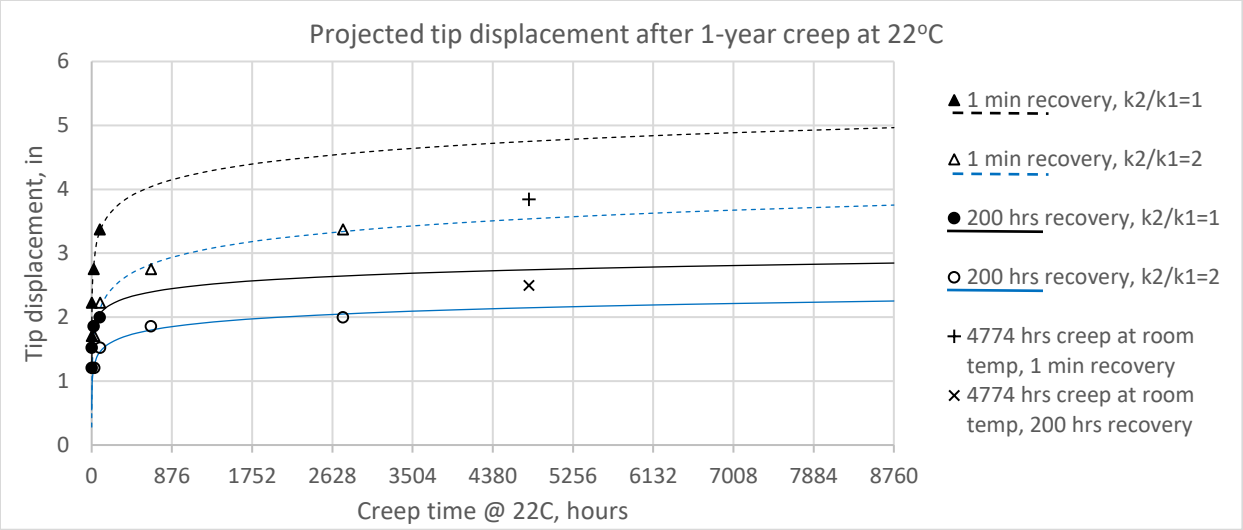

Fig. 8 Projected tip displacement versus room temperature creep duration

After 1 year (8760 hours) stowage at room temperature, it was concluded that given 200 hours of petal recovery (at room temperature), the residual tip deflection would be between 2.25 and 2.85 in; results of orbital thermal studies indicated that the average recovery temperature would be closer to 33° C which would decrease recovery time. At the onset of the creep investigation, two additional coupon samples were subjected to the same creep study and allowed to sit for nearly 200 days (4774 hours) at room temperature. The averaged deflection measurements after 1 minute and 200 hours are also plotted in Fig. 8 with hash marks "+" and "x" respectively. It is difficult to draw conclusions from single data points, however as expected, the values lie between the upper and lower bounds of k_2/k_1.

V. Flight Build and Delivery

As mentioned in section III above, the deployment architecture for this system relied on both the furling of the high strain composite petals on a central hub as well as the enclosure of the wrapped assembly into a 2U CubeSat volume. It was found that the simplest method for extracting this antenna system was to allow for the wrapped petals to pivot out of the cavity as a rigid body. Upon reaching full rotation, a tether would trigger the release of a restraint band that would enable the petals to be unfurled. To preload the wrapped petal assembly within the enclosure, a hold-down door, triggered by a mechanical release device, was also included. Upon door closure, the petals were sandwiched between the three walls of the CubeSat volume and the inner surface of the door. The compliance of the wrapped petal assembly minimized the need for careful shimming upon door preload. An overview of the system architecture is shown in Fig. 9 showing the door fully open and the wrapped petal assembly fully rotated out of the enclosure. The final step of deployment entails the release of the restraint band.

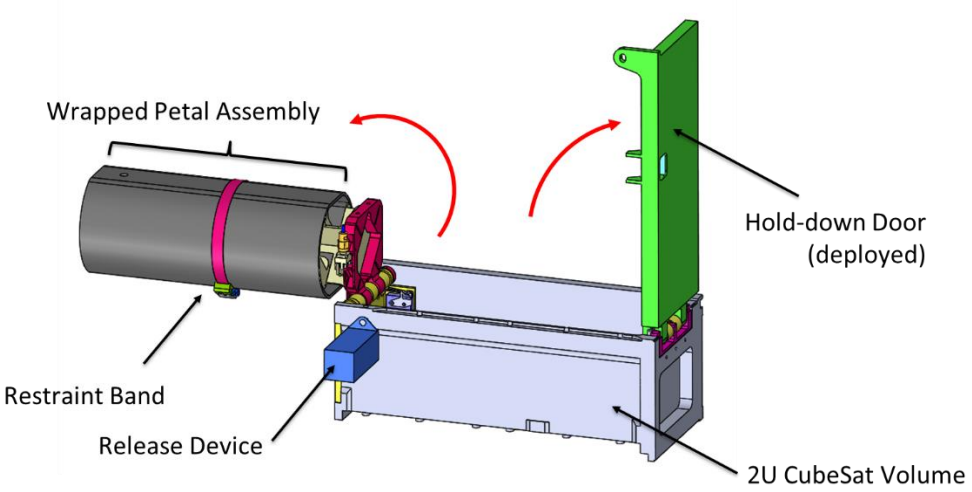

Fig. 9 Schematic overview of the petal deployment architecture in the configuration just prior to petal unfurling

The first prototype build of the full system occurred in December of 2016, four months after the kickoff of the program effort. The goal of this hardware, shown in Fig. 10, was to characterize system performance of the preliminary design and to buy down risk. Subsequent testing lead to the verification of several assumptions and requirements. Specifically the furled petals correctly acted as a single, flexible spring and with the closed door, provided reactive preload suitable to launch lock the system for flight. In addition the stowed dimensions of the furled wings and ability to freely deploy was found to meet expectations. Finally, the stowed force exerted on the restraint band was consistent with the value identified with the energy predictions. A few challenges however were first observed during this initial build. Of particular note was the debonding identified in the R0 region that led to the black oxide coating treatment to resolve the issues described in section IV. In addition, the creep effects of R0 and R1 led to laminate changes to mitigate / eliminate as described above in section III.

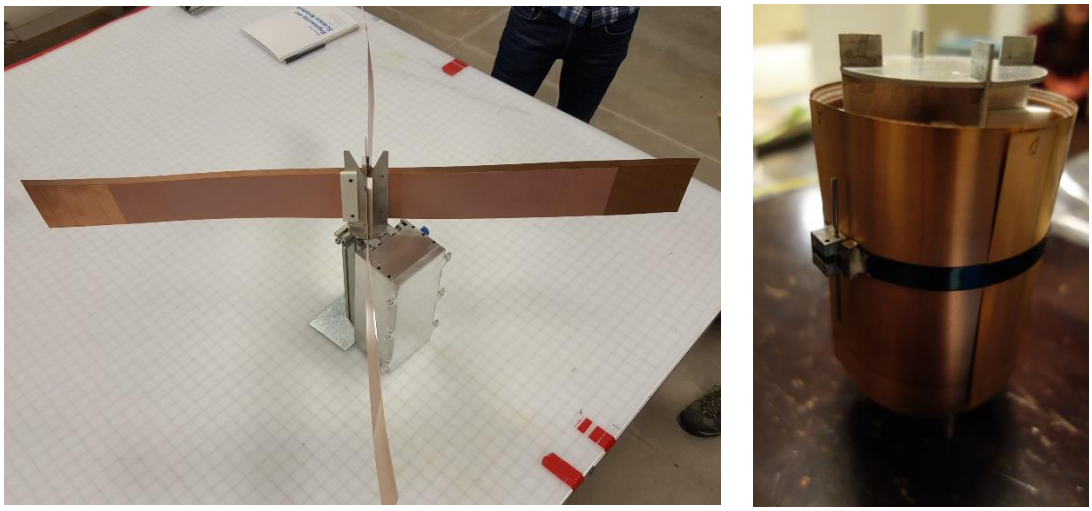

Fig. 10 Deployed prototype of winged structure deployed (left) and stowed (right)

The final flight system was fabricated in March of 2017 and successfully passed a suite of flight qualification testing including vibration and stow / deploy cycles at the extreme operational temperatures. The system, shown in Fig. 11, was found to be robust after multiple stow and deployment cycles however did show signs of wear-and-tear (abrasion marks, roughening of edges, etc.) after successive deployment cycles. This was mainly due to the difficulty in offloading the petals during the deployment testing and the inter-petal rubbing during the stowage process. As such the flight units were subjected to a limited number of full unfurling tests as part of the acceptance testing checkout.

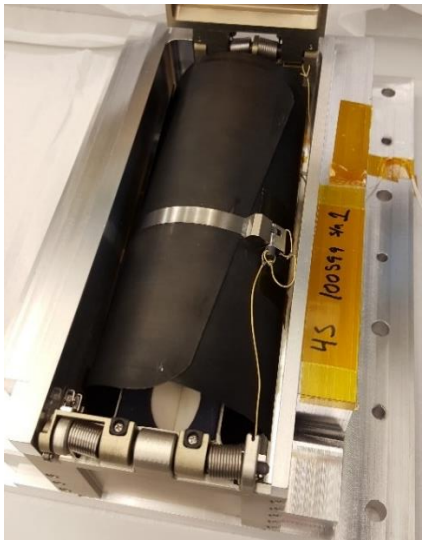

Fig. 11: Flight system, partially stowed (lid deployed) prior to flight vibration testing

VI. Conclusions

In Q3 of 2016, Roccor was approached to develop a CubeSat deployable antenna that would deploy four large radial petals while housed in a small, 2U volume. It was found that High Strain Composites coupled with a copper-beryllium alloy enabled a simplistic furled solution to stow the system with few mechanical parts. Optimization studies were performed to maximize the deployed petal natural frequency with respect to minimizing mass, laminate thickness, strain and creep susceptibility. Based on the final laminate architecture, strain energy was calculated for the stowed petals including spanwise variations in petal width, laminate design (layup and ply drop locations), and strain. During prototype fabrication, debonding issues arose between the copper-beryllium and glass fiber laminate. The issue was resolved by coating the CuBe with a black oxide which resulted in excellent interlaminar bonding. A top-level creep study was performed on the copper-beryllium/fiberglass-epoxy composite to estimate deployed petal precision after long-term creep. Though based on a small sample size of material test data, the results indicated robust performance with respect to tip position requirements and material degradation. Roccor delivered two, low-cost flight qualified units to the customer after a design, prototype, build and test campaign lasting a total of nine months. The hardware is slated to fly in early 2018.

References

[1] Zurbuchen T. H., et. al., "Achieving Science with CubeSats: Thinking Inside the Box," *National Academies of Sciences, Engineering, and Medicine*, 2016, Washington, DC, The National Academies Press. doi:10.17226/23503.

[2] Murphey, T. W., Francis, W. H., Davis, B. L., Mejia-Ariza, J. M., "High Strain Composites," *Proceedings of the 2nd AIAA Spacecraft Structures Conference, 2015 AIAA SciTech Conference, Session on Composite Materials for Spacecraft Structures*, AIAA 2015-0942, Kissimmee, FL.

[3] Reddy,J.N., *Mechanics of Laminated Composite Plates and Shells: Theory and Analysis*, 2nd ed. Boca Raton, Florida, USA: CRC Press, 2004.

[4] Lebbai, M., Kim, JK., Szeto, W.K., Yuen, M.F., Tong, P., "Optimization of Black Oxide Coating Thickness as an Adhesion Promoter for Copper Substrate in Plastic Integrated-Circuit Packages," *Journal of Electronic Materials*, Vol. 32, no. 6, 2003, pp 558 – 563.

[5] Domber, J.L, Hinkle, J.D., Peterson, L.D., Warren, P.A., "Dimensional Repeatability of an Elastically Folded Composite Hinge for Deployed Spacecraft Optics," *Journal of Spacecraft and Rockets*, Vol. 39, No. 5, September-October 2002.
[6] Fernandez, J.M., Banik, A.J., Ardelean, E.V., "Creep Effects and Deployment Characterization of Rollable Composite Shell Reflectors," *53rd AIAA/ASME/ASCE/AHS/ASC Structures, Structural Dynamics and Materials Conference*, Honolulu, HI, 23-26 April 2012. DOI: 10.2514/6.2012-1955.
[7] ASTM Standard F1980-16, *Standard Guide for Accelerated Aging of Sterile Barrier Systems for Medical Devices*, ASTM International, West Conshohocken, PA, 2016, www.astm.org. DOI: 10.1520/F1980-16.